https://doi.org/10.5194/egusphere-2024-3201
Preprint. Discussion started: 25 November 2024

Significant influence of oxygenated volatile organic compounds on atmospheric chemistry analysis: A case study in a typical industrial city in China

Jingwen Dai [a], Kun Zhang [a, *], Yanli Feng [a], Xin Yi [a], Rui Li [1], Jin Xue [a], Qing Li [a], Lishu Shi [a], Jiaqiang Liao [a], Yanan Yi [a], Fangting Wang [a], Liumei Yang [a], Hui Chen [a], Ling Huang [a], Jiani Tan [a], Yangjun Wang [a], Li Li [a, *]

[a] School of Environmental and Chemical Engineering, Shanghai University, Shanghai, 200444, China

Correspondence: Li Li (Lily@shu.edu.cn) and Kun Zhang (zk1231@shu.edu.cn)

Abstract

Oxygenated volatile organic compounds (OVOCs), key components of volatile organic compounds (VOCs), are either directly emitted or secondary generated via photochemical processes, and play a crucial role in tropospheric photochemistry and act as important ozone (O_3) precursors. However, due to measurement limitations, the influence of OVOCs on O_3 formation has often been underestimated. In this study, 74 VOCs (including 18 OVOCs) were measured at five representative stations in Zibo, an industrial city in the North China Plain. The VOCs level in Zibo (44.6±20.9 ppb) is in the upper-middle range compared with previous studies, with OVOCs contributing 30.0%~37.8% to the total VOCs concentration. The overall O_3 formation potential in Zibo is 410.4±197.2 μg m^{-3}, with OVOCs being the dominant contributor (31.5%~55.9%). An observation-based model (OBM) was used to access the contributions of chemical production ($R_{NetProd}$) and emissions/transport ($R_{Emis\&Trans}$) to individual OVOC. Daytime $R_{NetProd}$ is the highest at the urban site (5.9 ppb h^{-1}), while nighttime $R_{Emis\&Trans}$ is most significantly negative at the industrial site (0.76 ppb h^{-1}). Simulations without OVOCs constraint overestimates OVOCs (42.1%~126.5%) and key free radicals (e.g., HO_2

https://doi.org/10.5194/egusphere-2024-3201
Preprint. Discussion started: 25 November 2024

(5.3%~20.4%) and RO_2 (6.6%~35.1%)), leading to a 1.8%~11.9% overestimation of O_3. This overestimation causes an underestimation of OH (1.8%~20.9%) and atmospheric oxidizing capacity (3.5%~12.5%). These findings emphasize the importance of comprehensive OVOCs measurements to constrain numerical models, especially in regions with dense anthropogenic emissions, to better reproduce atmospheric photochemistry, and to formulate more effective air pollution control strategies.

1. Introduction

Oxygenated volatile organic compounds (OVOCs), contributing 20.1%~73.5% of total volatile organic compounds (VOCs) (Han et al., 2019; Huang et al., 2020; Li et al., 2022a; Liu et al., 2024; Song et al., 2024), are critical components of tropospheric photochemistry (Yang et al., 2014). Photolysis of OVOCs has been proved to be the most significant primary source of RO_x (OH + HO_2 + RO_2) in Guangzhou, Beijing, and Xi'an in China (Wang et al., 2022; Yang et al., 2018; Zhang et al., 2021b), and thereby accelerating the recycling of radicals to promote ozone (O_3) formation (Qu et al., 2021; Wang et al., 2022). In addition, previous studies have shown that sufficient free radicals produced by photolysis of OVOCs are the dominated contributors to O_3 pollution during winter (Edwards et al., 2014; Emmerson et al., 2005). For example, the study of Li et al. (2021b) indicates that the fast generation of O_3 during winter haze in the North China Plain is mainly driven by the photolysis of formaldehyde (HCHO), which leads to more productions of HO_x radical and offsets the radical titration induced by NO_x emissions. In addition, HCHO and other OVOCs dominated the OH loss with VOCs (Goldan et al., 2004), resulting in predominant role in OH reactivity (Ling et al., 2014; Yang et al., 2018). Therefore, OVOCs play a significant role in the atmospheric chemistry. OVOCs have complex sources, including primary emissions from anthropogenic and natural

https://doi.org/10.5194/egusphere-2024-3201
Preprint. Discussion started: 25 November 2024

sources, as well as secondary formation through photochemical reactions (Huang et al., 2020; Song et al., 2024; Xia et al., 2021). For instance, Mo et al. (2016) estimated that OVOCs from heavy-duty diesel vehicle emissions accounted for 53.8% of total VOCs in China, and OVOCs account for 12.4%~46.3% of VOCs emission from biomass and residential coal combustion, which demonstrates the importance of combustion-related sources of OVOCs. In addition, measurement of VOCs fluxes based on the airborne eddy covariance technique showed that urban emission sources comprise a surprisingly large proportion of OVOCs (29%~56%) (Karl et al., 2018; Pfannerstill et al., 2023).

Chemical transport models (CTMs) have been widely used for the study of formation mechanism of OVOCs and their influence on air quality (Chen et al., 2022; de Gouw et al., 2018; Luecken et al., 2012; Steiner et al., 2008; Yang et al., 2023). However, due to the deviation of the meteorological field, uncertainty of the emission inventory (Li et al., 2019; McDonald et al., 2018; Shen et al., 2019), defects of lumped chemical mechanism (Li et al., 2014a; Sarwar et al., 2008; Stockwell et al., 1997a; Venecek et al., 2018), uncertain secondary generation source (Koss et al., 2015; Liu et al., 2015), unknown dilution and transport process (Wolfe et al., 2016), and the negligence of the primary emission of OVOCs (Li et al., 2014b), there is a large uncertainty in the OVOCs simulated by CTMs, which in turn leads to large deviations in the simulated atmospheric photochemistry. The observation-based model (OBM) can avoid these biases to a certain extent by constraining meteorological parameters and chemical species, and leveraging detailed chemical mechanism (e.g., Master chemical mechanism, MCM). Nevertheless, due to the limited observations of OVOCs (e.g., Pfannerstill et al., 2023), many existing studies use OBM without the observed OVOCs data, or only with limited inputs for certain OVOCs species (formaldehyde,

https://doi.org/10.5194/egusphere-2024-3201
Preprint. Discussion started: 25 November 2024

acetaldehyde, acetone), which can greatly bias the assessment of O_3 generation mechanism, free radical chemistry, and atmospheric oxidation. For instance, Wang et al. (2022a) showed that the box model without the constraint of OVOCs underestimates the OVOCs concentrations, which in turn lead to the underestimation of RO_x and O_3 formation. Thus, it is meaningful to couple OVOCs observation with OBM to investigate how OVOCs affect radical chemistry, atmospheric oxidization capability, and O_3 formation mechanism.

Zibo, a typical industrial cluster city in China, has been suffering from O_3 pollution for years (Li et al., 2021a; Qin et al., 2023). However, comprehensive studies involving the observation of VOCs, particularly OVOCs such as HCHO, are rare in this city. For instance, Qin et al. (2023) used observations of 98 VOCs (without HCHO) in Zibo to constrain OBM, but the absence of HCHO in their simulation could result in underestimation RO_x, thus disturbing the investigation of OH budget (Fuchs et al., 2017; Guo et al., 2021; Ling et al., 2014; Qu et al., 2021; Tan et al., 2017). In this study, a 5-day field campaign was conducted across five representative sites in Zibo. Concentrations of 74 VOC species including 18 OVOCs (e.g., formaldehyde, acetaldehyde, and acetone) are obtained. The contributions of secondary formation, emissions/transport to OVOCs level are analyzed by OBM model. Additionally, the impact of OVOCs on radical chemistry, atmospheric oxidation capability, and consequently O_3 production are quantified.

2. Methodology

2.1 Sampling sites and measurements

To capture a typical ozone pollution case, the field campaign was conducted from August 8 to August 12, 2021, at five monitoring sites (Zhonglou (ZL), Chengdong (CD), Chengqu (CQ), Tianzhen (TZ), and Xindian (XD)) in Zibo (Figure 1, Table S1). Among the five sites, ZL site

https://doi.org/10.5194/egusphere-2024-3201
Preprint. Discussion started: 25 November 2024

(117°54'E, 36°39'N) is an urban site, which is located in the central area of Zibo, and is mainly surrounded by residential areas and factory buildings. According to the prevailing wind direction (northeast, Figure S1 (a)), CQ (118°60'E, 36°57'N) site is an upwind site, while CD (117°53'E, 36°31'N) is a downwind site. CD is located on a hillside in the southern part of Zibo, with a small number of ceramic and refractory enterprises factories neaby. TZ (117°48'E, 37°10'N) is close to Shengli Oil field on the west, and is surrounded by farmland. This site is regarded as a suburban site and is affected by residential emissions in the north of Zibo and oil production operations. XD (118°19'E, 36°48'N) is close to a chemical industrial park and serves as an industrial site. More detailed information about these sites can be found in Table S1.

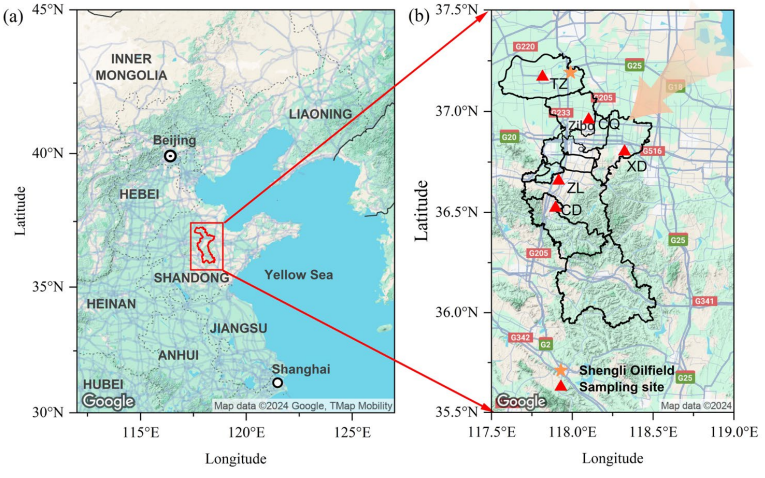

Figure 1. (a) Map of the North China Plain and (b) map of Zibo with locations of VOCs monitoring stations (red triangles), and Shengli Oil field (yellow star), and prevailing wind direction (orange arrow).

During the campaign, two online gas chromatography-flame ionization detector (GC-FID, Thermo Scientific GC5900) systems were deployed at suburban (TZ) and upwind (CQ) stations, and three online gas chromatography-flame ionization detector (GC-FID, Syntech Spectras GC 955–615/815) systems were deployed at downwind (CD), industrial (XD) and urban (ZL) stations, respectively. A total of 56 VOCs (PAMS), including 29 alkanes, 16 aromatics, 10 alkenes and

https://doi.org/10.5194/egusphere-2024-3201
Preprint. Discussion started: 25 November 2024

acetylene, were measured by each VOCs analyzer with 1-hour resolution. Additionally, 18 oxygenated VOCs species were collected by 2,4-dinitrophenylhydrazine (DNPH) sorbent tubes in conjunction with an automated sampler for a period of 1 or 3 hour per sample. A total of 271 valid OVOCs samples were collected during the campaign. At the industrial (XD) and suburban (TZ) stations, 8 samples were collected per day at 3-hour intervals, with 47 valid samples at each station. At the urban (ZL), upwind (CQ) and downwind (CD) stations, 10 samples were collected per day, with 7 samples collected at 1-hour intervals during 7:00-21:00 LT, and 3 samples collected at 3-hour intervals during the night (1:00-6:00 and 22:00-1:00^{+1} LT), and totaling 59 valid samples per station. The OVOCs samples were first eluted with acetonitrile to elute the derivatives and then analyzed by an off-line high performance liquid chromatography (HPLC) system. Finally, a total of 74 VOCs were combined to conduct data analysis in this study. Conventional gas phase pollutants (e.g., O_3, CO, and NO_x (NO and NO_2)) were measured using commercial online analyzers (Thermo Scientific 49i, 48i, and 42i, USA) at each site. NO_x was measured by NO chemiluminescence and chemical conversion with a molybdenum convertor, which is known to be interfered by NO_z species (Tan et al., 2017, 2019a). Meteorological parameters, including temperature (T), relative humidity (RH), wind speed (WS), wind direction (WD), and ambient pressure (P) were obtained synchronously by Chinese ground-based meteorological stations (Boshan, Huantai, Gaoqing, Linzi, and Zichuan sites) (http://data.cma.cn/, last access: March 26, 2024).

2.2 Observation-based model

A box model (F0AM) coupling with Master Chemical Mechanism (MCM) v3.3.1 was utilized to simulate the in situ atmospheric chemical process at these 5 sites (Jenkin et al., 2015; Wolfe et al., 2016). The MCMv3.3.1 is a nearly explicit mechanism with more than 5800 species and 17000

https://doi.org/10.5194/egusphere-2024-3201
Preprint. Discussion started: 25 November 2024

reactions, which is able to describe more detailed gas chemistry than other lumped mechanisms, such as Carbon Bond Mechanism (CB) (Yarwood et al., 2005, 2010), Regional Atmospheric Chemistry Mechanism (RACM) (Goliff et al., 2013; Stockwell et al., 1997b), and SAPRC (Carter, 1990, 2010; Carter and Heo, 2013). The box model calculations were constrained by measured trace gases, including NO and NO_2, CO, SO_2, and 45 speciated VOCs, including 20 alkanes, 11 alkenes, 14 aromatics, and 15 OVOCs, as well as meteorological parameters, including T, RH and P. HONO was fixed to 2% of the NO_2 mixing ratio (Elshorbany et al., 2012; Tan et al., 2019a). H_2 was assumed to be 550 ppb (Lou et al., 2010). In addition, boundary layer height (BLH), and surface net solar radiation (SSR) were obtained from the fifth generation of the European Centre for Medium-Range Weather Forecasts (ECMWF) reanalysis for the global climate and weather (https://cds.climate.copernicus.eu, last access: March 1, 2024). The photolysis frequency correction factor (Jcorr) of the model input was adjusted by SSR. BLH was also included in the model to control the deposition process (Xuan et al., 2023; Zhu et al., 2020).

The model ran with continuous time series profile for the campaign period (August 8-12) with 1-hour resolution. Each simulation starts with 10-days spin up to reach steady state condition. Missing observation data were filled with linear interpolation, and the concentrations of OVOCs were also linearly interpolated to 1-hour resolution for modeling. An artificial loss process corresponding to an atmospheric lifetime of 24 h or a first-order dilution rate (kdil) of 1/86400 s^{-1} was introduced for all simulated species, including secondary species and radicals, to approximately simulate dry deposition and other losses (Lou et al., 2010; Tan et al., 2018b; Wang et al., 2022). The model cases that run with the above settings with 15 constrained OVOCs species are called the Base scenario. To investigate the impacts of constrains of OVOCs on atmospheric chemistry, the Free

https://doi.org/10.5194/egusphere-2024-3201
Preprint. Discussion started: 25 November 2024

scenario (Table S2) was conducted with the setting of the Base scenario excluding OVOCs constrain.

According to previous studies, the variation of OVOCs mixing ratios is mainly influenced by in-situ photochemical production, emissions and regional transport, and deposition (Tan et al., 2018a; Xue et al., 2014). The change rate of observed OVOCs (R_{Meas}) is calculated by the derivative of the measured OVOCs concentrations, as shown in Equation (1). The local net OVOCs photochemical production ($R_{NetProd}$) and the removal of OVOCs by deposition (R_{Dep}) are calculated hourly according to the OBM simulation. The emissions and regional transport of OVOCs ($R_{Emis\&Trans}$) are computed as Equation (2).

$$R_{Meas} = \frac{d(OVOC)}{dt} \quad (1)$$

$$R_{Emis\&Trans} = \sum \left(R_{Meas} - R_{NetProd} - R_{Dep}\right) \quad (2)$$

3. Results and discussion

3.1 Meteorological and chemical conditions

The field campaign is characterized by consistent hot and sunny conditions, with an average daytime maximum temperature of 32.3 °C (peak at 34.1 °C) (Figure 2). A typical O_3 episode was observed, with an average maximum daily 8-hour average O_3 (MDA8-O_3) of 89.8 ppb in Zibo city. According to the Chinese National Ambient Air Quality Standard Grade II (about 93.3 ppb for 1-hour average, or 74.7 ppb for maximum daily 8-hour average (MDA8-O_3)), there are four O_3 pollution days (August 8 to 11) during the campaign. The average mixing ratios of SO_2, NO_2, NO, and CO in Zibo are 2.8±1.6, 12.0±6.9, 2.8±4.8, and 897±670 ppb, respectively (Figure 2, Figure S2 (b)). The mean VOCs concentration in this study is 44.6±20.9 ppb, which is overall higher than that in Beijing (18.3±8.9 ppb) from July 23 to August 31 in 2016 (Wu et al., 2023), Rizhao (9.83 ppb) in summer in 2022 (Zhang et al., 2023), and Xi'an (29.1± 8.4 ppb) from June 20 to July 2019 (Song

https://doi.org/10.5194/egusphere-2024-3201
Preprint. Discussion started: 25 November 2024

et al., 2021). Compared with urban areas in other cities (Figure S3, Table S3), VOCs level at ZL is in the upper middle range, indicating strong anthropogenic VOCs emission at Zibo city. In terms of the VOCs groups (Figure S4 (a)), alkanes and OVOCs were the two predominant groups at each site, accounting for 33.3~51.5% and 30.0~37.8% to the total VOCs, respectively, followed by aromatics (3.8~16.5%) and alkenes (5.0~13.8%). During the campaign, the average daily maximum temperature and SSR was 32.2±1.4 ℃ and 2.1±0.4×10^6 J m^{-2} (Figure S2 (a)), respectively, which favors the photochemical formation of O_3. In addition, the difference between peak and valley NO_2 concentrations was 14.4±3.2 ppb, indicating that substantial NO_x was converted to O_3.

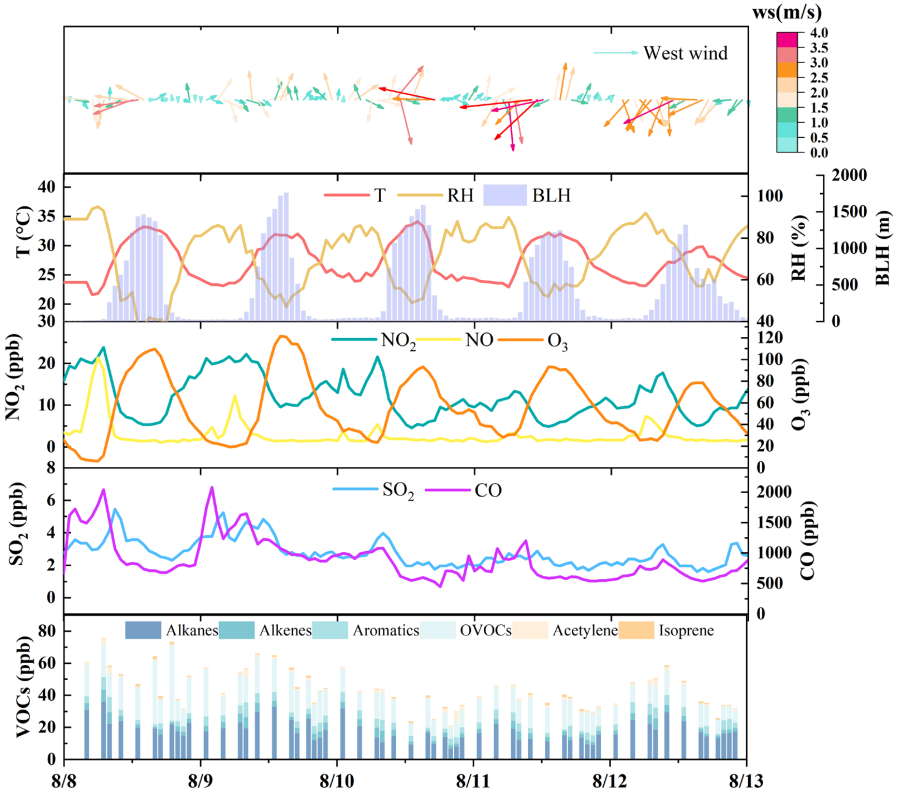

Figure 2. Time profiles of pollutant mixing ratios and meteorological parameters in Zibo from August 8 to 12, 2021. The meteorological data were from ZL, the central site of Zibo, and the pollutants data were the average of the five sites. The timing of the PAMS data was matched to that of the OVOCs data.

https://doi.org/10.5194/egusphere-2024-3201
Preprint. Discussion started: 25 November 2024

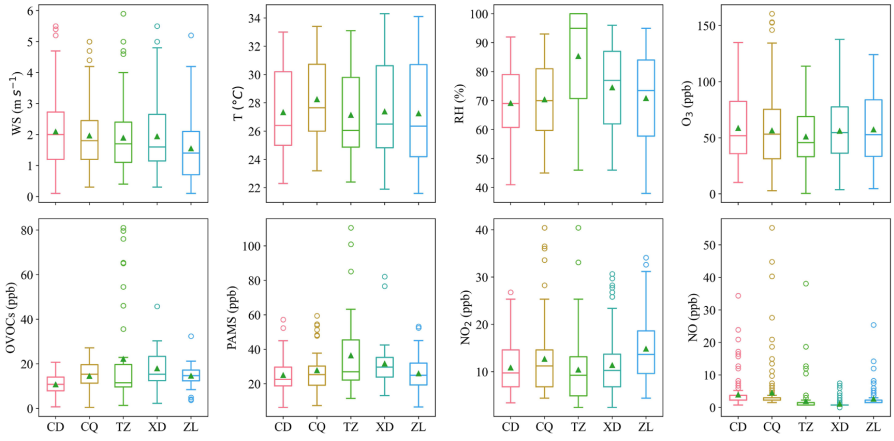

Figure 3. Distribution of O_3 and its precursors (OVOCs, PAMS, NO_2, and NO) and meteorological parameters (WS, T, and RH) at five sites, with the green triangle being the mean value and the horizontal line in the box being the median. The summary of those parameters is listed in Table S4.

As for individual site, the average O_3 concentration are comparable across the downwind site (CD, 58.6±30.0 ppb), urban site (ZL, 57.4±32.2 ppb), upwind site (CQ, 56.4±34.2 ppb), and industrial site (XD, 56.1±29.4 ppb), with the suburban site (TZ, 51.0±27.8 ppb) being slightly lower (Figure 3). TVOCs at suburban site (TZ, 58.5±35.0 ppb) is the highest (Figure 3, Table S4), followed by industrial site (XD, 49.6±19.0 ppb), while the upwind site (CQ, 42.3±15.4 ppb) and urban site (ZL, 40.6±10.3 ppb) have comparable levels. As mentioned above, TZ is close to the Shengli Oil field, and there are many oil refineries near this site, which is consistent with the high VOCs concentrations at this site. Although the downwind site (CD) has slightly lower NO_2 level (10.8±5.1 ppb) and lower TVOCs concentration (35.7±12.5 ppb) than upwind site (CQ, 12.7±8.1 ppb and 42.3±15.4, respectively), the O_3 concentrations (58.6±30.0 ppb) is higher than that at upwind site (56.4±34.2 ppb). This may be attributed to the transport of O_3 and its precursors from northeastern (Figure S1).

According to the time series of individual pollutant (Figure S2 (b)), CQ showed obvious peak concentrations of O_3, NO_2, NO and CO than the other sites during August 8-9, with stagnant

https://doi.org/10.5194/egusphere-2024-3201
Preprint. Discussion started: 25 November 2024

conditions (WS < 2 m s^{-1}), indicating stronger emissions associated with combustion sources and possibly accompanied by fast photochemical reaction process near CQ. In addition, XD showed significant high mixing ratios of CO during August 8~9, and relatively high concentrations of TVOCs during the daytime on August 9 (9:00-14:00 LT, 90~110 ppb). Since CO is relatively inert and no similar CO peak was found at the other 4 sites, we believe the abnormal CO peaks at XD are related to strong emissions from neighboring factories in the industrial park. TZ showed a significant morning and evening peak of TVOCs at 6:00 LT (163.0 ppb) and 21:00 LT (120.0 ppb) on August 8, and a night peak at 1:00 LT on August 10 (130.3 ppb), which were related to emissions from the neighboring oil field operations. During August 10-12, the wind speed gradually became faster, and the mixing ratios of pollutants at each site decreased to similar level. Overall, the local anthropogenic emissions in Zibo were more prominent when the wind was weak.

To compare the secondary O_3 formation in each site, the ozone formation potential (OFP) of each VOCs is calculated. The mean OFP in Zibo during the observation is 410.4±197.2 μg m^{-3}, with OVOCs accounting for the largest proportion (31.5%~55.9%). As for individual site, the upwind station (CQ, 464.2±162.3 μg m^{-3}) has the highest OFP, followed by the suburban site (TZ, 456.3±295.3 μg m^{-3}), the urban site (ZL, 441.1±174.5 μg m^{-3}), the industrial site (XD, 422.9±166.9 μg m^{-3}), and the downwind site (CD, 279.4±101.2 μg m^{-3}). Apart from CQ, OVOCs are the dominant contributors to OFP at each site, especially TZ and XD, with mean OFP of 254.9±276.1 μg m^{-3} (55.9%) and 194.7±101.0 μg m^{-3} (46.0%) from OVOCs, respectively. This indicates the kay role of OVOCs in the formation of O_3 at our observational sites. Among OVOCs, HCHO is the dominant contributor to OFP across the five sites (56.6~202.0 μg m^{-3}). This is consistent with previous studies (Duan et al., 2008; Huang et al., 2020; Zhou et al., 2024). Additionally, the variety of VOCs sources,

https://doi.org/10.5194/egusphere-2024-3201
Preprint. Discussion started: 25 November 2024

meteorological condition, and photochemical condition in each site lead to differences in key species of OFP at each site. At the suburban site (TZ), isoprene (34.9 μg m^{-3}) ranks 2nd in terms of OFP after formaldehyde (202.0 μg m^{-3}), indicating a high impact of biogenic emissions (Mo et al., 2018; Sindelarova et al., 2014). At the industrial site (XD), the contribution of isopentane, marker of oil and gas emissions, to OFP is more prominent (as high as 66.2 μg m^{-3}) than other sites. OFP of highly reactive aromatic hydrocarbon species, such as m/p- xylene (53.8 μg m^{-3}) and o-xylene (23.6 μg m^{-3}) are predominant at upwind site (CQ), indicating outstanding contribution of solvent-using sources. OFP contributed by alkenes is the highest at urban site (101.8±56.8 μg m^{-3}) (Figure 4 (a)), with ethylene and propylene being the most key species, which is consistent with the dense vehicle emission near this site.

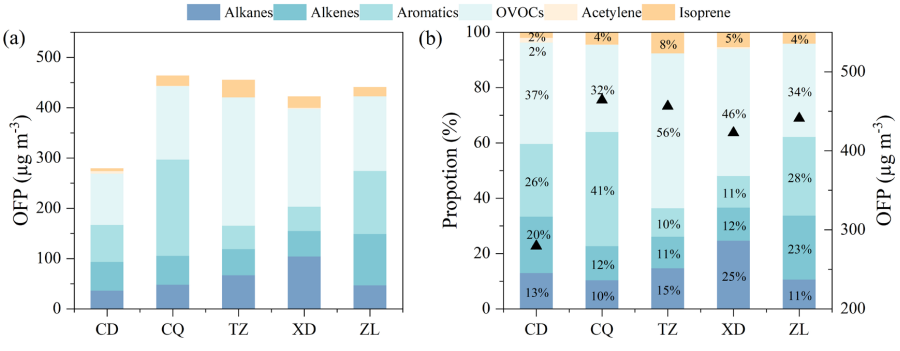

Figure 4. Concentrations (a) and proportions (b) of OFP contributed by VOCs components at five sites.

3.2 Contribution of chemical generation, emissions/transport to OVOCs

To separate the contribution of secondary formation, emissions/transport to OVOCs, OBM analysis is occupied. Overall, all five sites show good model performance in base case. The R values at the five sites are higher than 0.85, and IOA values are all greater than 0.80 (Figure S5), which is comparable to previous studies (Qin et al., 2023; Zheng et al., 2023). According to Xue et al. (2014), the net photochemical production rate of OVOCs ($R_{NetProd}$), contribution of emission/transmission

https://doi.org/10.5194/egusphere-2024-3201
Preprint. Discussion started: 25 November 2024

on OVOCs ($R_{Emis\&Trans}$) and OVOCs deposition rate (R_{Deps}) is calculated based on OBM results. The measured variation of OVOCs concentration (R_{Meas}) is calculated by the derivative of the measure OVOCs concentrations (R_{Meas} = d(OVOCs)/dt), and it equals to the sum of $R_{NetProd}$, $R_{Emis\&Trans}$ and R_{Deps} (Equation (1) and (2)). The net secondary generation of OVOCs at each station mainly concentrated in the daytime (Figure 5). The maximum average daytime $R_{NetProd}$ of OVOCs was observed at ZL (5.9±3.5 ppb h^{-1}), followed by CQ (4.11±11.9 ppb h^{-1}), XD (3.6±2.4 ppb h^{-1}), CD (3.5±2.0 ppb h^{-1}) and TZ (1.9±3.6 ppb h^{-1}) sites. This suggests that abundant reactive VOCs emissions at urban areas as well as in the industrial areas could lead to faster generation of OVOCs. Generally, the $R_{NetProd}$ varied with a single peak due to photochemical formation and export transport, with the maximum value at 12:00-14:00 LT. The mean peak of $R_{NetProd}$ at ZL was 8.8 ppb h^{-1}, followed by XD (5.6 ppb h^{-1}), CQ (5.5 ppb h^{-1}), CD (5.1 ppb h^{-1}) and TZ (3.0 ppb h^{-1}). Generally, in the early morning hours (4:00-10:00 LT), positive R_{Meas} at CD, CQ, and XD sites are driven by $R_{Emis\&Tran}$ import. During this period, OVOCs concentrations show a significant upward trend, peaking between 8:00 and 10:00 LT.

Overall, OVOCs concentrations at CD, CQ, and ZL sites were typically lower at night but higher during the daytime (Figure 5 (a)), attributing to strong daytime photochemical generation, especially at around 7:00-10:00 LT. In contrast, TZ and XD showed higher nighttime OVOCs than that at daytime, which is due to stronger emission import during night. In addition, though $R_{NetProd}$ at ZL was the fastest during the daytime, the airmass transport can efficiently export OVOCs to unwind areas, leading to relatively lower OVOCs concentrations. While at TZ, $R_{NetProd}$ was the lowest, but the daytime OVOCs was the highest due to the predominant daytime import, especially the southwestward import on August 8 (Figure S6 (c)).

https://doi.org/10.5194/egusphere-2024-3201
Preprint. Discussion started: 25 November 2024

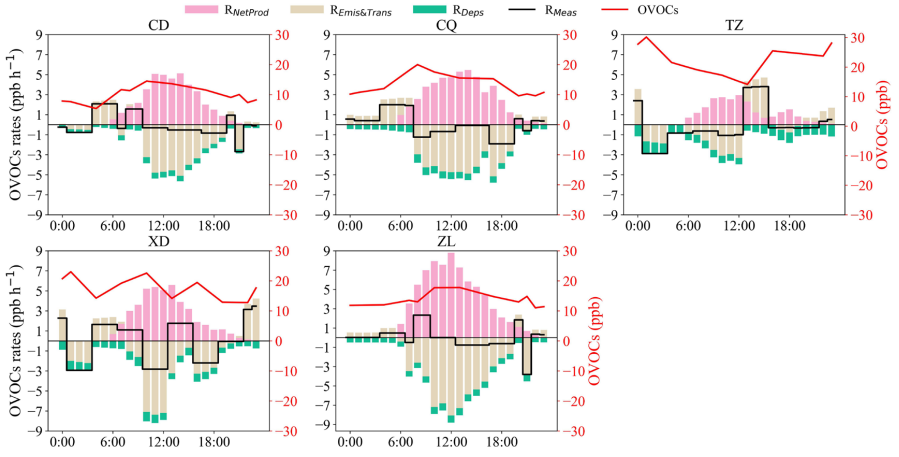

Figure 5. (a) Diurnal profiles of OVOCs contributions from local photochemical production ($R_{NetProd}$), deposition (R_{Deps}), emission/transport ($R_{Emis\&Trans}$), and measured O_3 formation rate (R_{Meas}) and (b) time profiles of $R_{Emis\&Trans}$ of the five sites.

3.3 Importance of OVOCs observationally constraint in OBM

To investigate the effect of the constrain setting of OVOCs on OBM performance, the simulated OVOC, O_3, radicals in the Free and Base scenarios are compared (Figure 6). It has been shown that the box model, which did not take into account transport (including horizontal and vertical diffusion) and emissions, will results overestimations of OVOCs, peroxyl radical and PAN (Qu et al., 2021). In this study, OVOCs are overestimated by 42.1%~126.5% in the Free scenario (Figure 6 (a), Figure S7 (c)), especially HCHO (76.3%) and benzaldehyde (737.5%). The daytime RO_x was overestimated by 6.5%~23.3%, with RO_2 and HO_2 being overestimated by 6.6%~35.1% and 5.3%~20.4%, respectively, while OH was underestimated by 1.8%~20.9% (Figure 6 (d-f), Figure S8 (b)). As shown in Figure 7 (a), photolysis of OVOCs (include HCHO) is the predominant source of RO_x radicals ($P(RO_x)$) in the daytime, which is consistent with the findings in Beijing (Liu et al., 2012), Shanghai (Zhang et al., 2021a), Hong Kong (Xue et al., 2016), and Mexico (Volkamer et al., 2010). To have an insight of the impact of OVOCs on RO_x simulation, the known chemical budgets of RO_2, HO_2, and OH are quantified according to Liu et al. (2012) and Xue et al. (2016)

https://doi.org/10.5194/egusphere-2024-3201
Preprint. Discussion started: 25 November 2024

(Figure 7 (b), Figure S9 (a)). The daytime net production of RO_x ($P(RO_x)$) in the Free scenario is 0.03~0.14 ppb h^{-1} at four sites (except TZ), which results in overestimation of RO_x. While it is negative at TZ site, possibly due to unknown RO_x sources. The simulated mean daytime $P(RO_x)$ in the Free scenario is 4.8±2.7 ppb h^{-1}, 18.8% higher than that in the Base scenario. As the daytime RO_x budget shown in Figure 7(b) and Figure S10, the photolysis of OVOCs (include HCHO) dominants $P(RO_x)$, with mean rate of 2.9±1.9 ppb h^{-1} in the Free scenario, which is 27.4% higher than that in Base scenario. Nevertheless, the interference of OVOCs on OH is comprehensive. On the one hand, the increase of OVOCs tends to elevate the generation of HO_2, which can directly or indirectly increase the production of OH via the reaction of NO (Figure S10). On the other hand, the higher OVOCs concentration can decrease OH via the reaction of OH+OVOCs (Qu et al., 2021; Tan et al., 2019b). In the Free scenario, the total sources (include H_2O_2+hv, HONO+hv, O_3+hv, and HO_2+NO) of OH is 7.9~12.1 ppb h^{-1}, which is 0.3~1.1 ppb h^{-1} higher than that in the Base scenario. However, the destruction of OH to peroxyl radicals in the Free scenario (7.1~11.8 ppb h^{-1}) is 0.4~2.2 ppb h^{-1} higher than that in Base scenario, leading to net loss of OH (0.1~0.9 ppb h^{-1}). Furthermore, this underestimation of OH without OVOCs constraint results in a notable biases of AOC (3.4%~12.7%) (Figure S11) as well, which can further affect the evaluation of VOCs decay via the oxidation of OH oxidation (Li et al., 2022b). As for individual site, in the Free scenario, RO_x production increased by 29.4% at urban site (ZL) (Figure 7 (b)) than the Base scenario, which is comparable to downwind site (CD) (27.6%), and significantly higher than that at industrial site (XD) (17.8%), upwind site (CQ) (15.8%), and TZ (4.7%). Particularly, the photolysis of HCHO is the most significant pathway effecting RO_x production in the Free scenario, with an increase of 7.8%~151.2% (0.1~1.2 ppb h^{-1}) than the Base scenario. As the daytime RO_x budget shown in Figure

https://doi.org/10.5194/egusphere-2024-3201
Preprint. Discussion started: 25 November 2024

7 (b) and Figure S9, the primary formation pathways of RO_x (OVOCs (include HCHO) photolysis) enhanced by 4.6%~44.4% at different sites, which is an important reason for the increase of peroxyl radicals.

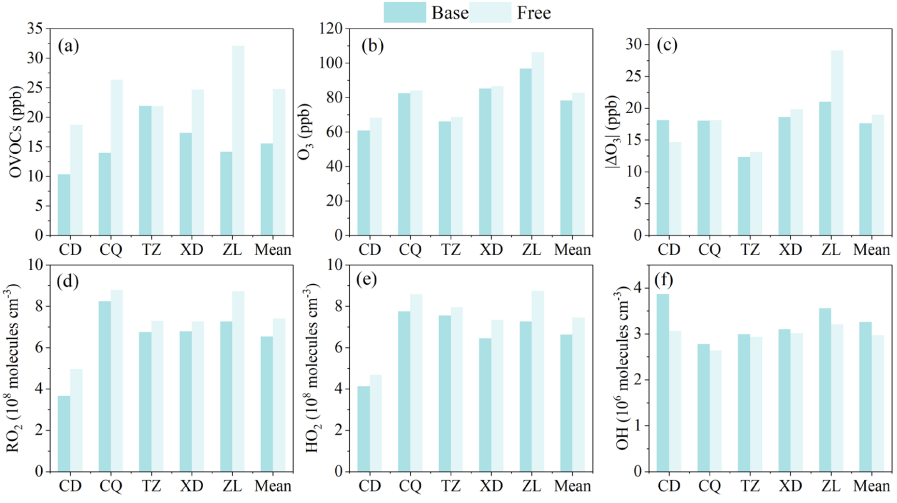

Figure 6. Comparison of average (a) OVOC, (b) daytime O_3, (c) daytime $|\Delta O_3|$ (the gap between simulated and observed daytime O_3 concentrations), and RO_x ((d) RO_2, (e) HO_2, and (f) OH) between the Base and Free scenario simulations.

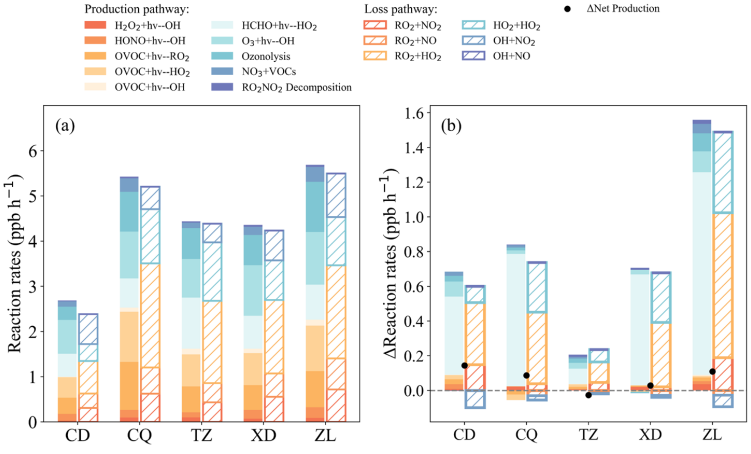

Figure 7. (a) Average daytime sources and sinks of RO_x in Base case and (b) the impact of OVOCs observationally constraints on RO_x budget, calculated by (Free - Base).

https://doi.org/10.5194/egusphere-2024-3201
Preprint. Discussion started: 25 November 2024

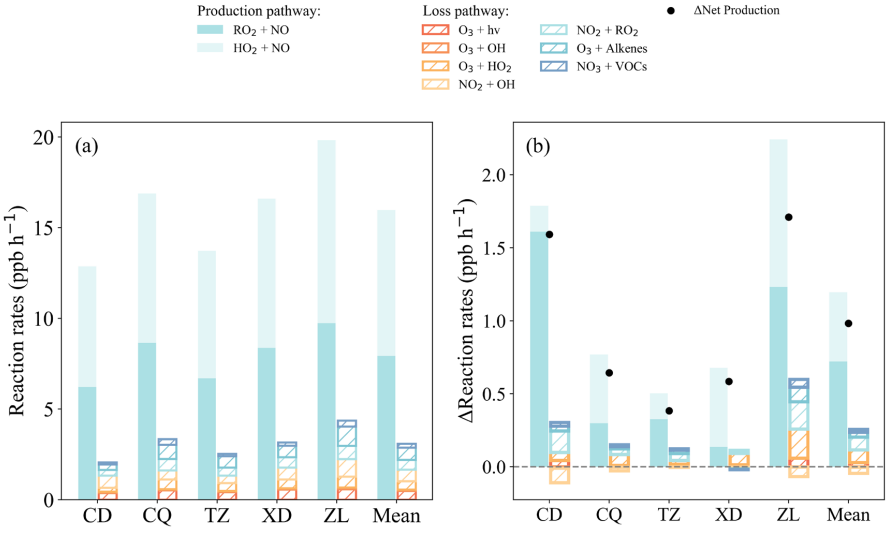

Figure 8. (a) Average daytime O_3 production and loss rates (ppb h^{-1}) in Base scenario and (b) the impact of OVOCs observationally constraints on O_3 budget, calculated by (Free - Base).

Overall, the gap between simulated and observed daytime O_3 concentrations ($|\Delta O_3|$) in the Free case increased by 7.5% compared to that in the Base scenario. To better understand the influence of OVOCs on O_3 formation, the rates of the main production and sink pathways of O_3 in the Base and Free scenarios are summarized (Figure 8, Figure S9 (b)). Compared to the Base scenario, the diurnal $P(O_3)$ in the Free scenario increases by 3.7%~13.9%, with the reaction rates of RO_2+NO and HO_2+NO increases by 1.6%~25.9% (0.1~1.6 ppb h^{-1}) and 2.5%~10.0% (0.2~1.0 ppb h^{-1}), respectively. This is attributed to the elevated RO_2 and HO_2 radical concentrations simulated without constraints of OVOCs observations (Figure 6 (d-e)). In contrast, the lower simulated concentration of OH radicals in the Free scenario results in a 0.5%~14.8% (0~0.1 ppb h^{-1}) decrease in the OH+O_3/NO_2 reaction rate. Although the $L(O_3)$ in the Free scenario is 0.4~1.7 ppb h^{-1} higher than that in the Base scenario, it cannot offset the increase of $P(O_3)$, leading to higher net product of O_3. Thus, no constraints of OVOCs could lead to overestimate peroxyl radicals in the OBM, which in turn significantly overestimates the deviation of O_3 due to the formation pathway of RO_2/HO_2+NO.

https://doi.org/10.5194/egusphere-2024-3201
Preprint. Discussion started: 25 November 2024

Of course, the impact of OVOCs varies considerably in different emission and functional regions. The simulated mean daytime O_3 in the Free scenario is 106.3, 86.7, 84.1, 68.8, and 68.2 ppb h^{-1} at ZL, XD, CQ, TZ, and CD, respectively, which is 9.8%, 1.8%, 2.0%, 3.9%, and 11.9% higher than that in the Base scenario (Figure 6 (b), Figure S7 (a), Table S5). The mean diurnal $|\Delta O_3|$ at ZL site (29.1 ppb, 38.2%) in the Free scenario was significantly higher compared to that of the Base scenario, followed by XD (19.8 ppb, 6.4%), TZ (13.1 ppb, 6.2%) and CQ (18.1 ppb, 0.6%) (Figure 6 (c), Table S5), suggesting that the absence of OVOCs constraint in OBM can significantly bias the O_3 formation analysis in urban and industrial areas with complex emissions.

4. Conclusions

Compared with previous studies, the VOCs level in Zibo is in the upper-middle range, with OVOCs being the second-largest contributor (29.4%~36.1%) after alkanes (34.8~53.3%). Higher levels of OVOCs were observed at sites with more prominent emissions, with OVOCs concentrations ranked as suburban (TZ, 19.7 ppb) > industrial (XD, 16.8 ppb) > urban (ZL, 14.9 ppb) > upwind (CQ, 13.9 ppb) > downwind (CD, 10.4 ppb). The OFP in Zibo is 367.9±208.5 μg m^{-3}, with OVOCs accounting for the largest proportion (40.1%). As for individual site, the upwind site (CQ, 485.7±212.2 μg m^{-3}) has the highest OFP, followed by the urban site (ZL, 443.2±173.9 μg m^{-3}), the suburban site (TZ, 418.8±282.4 μg m^{-3}), the industrial site (XD, 397.0±166.8 μg m^{-3}), and the downwind site (CD, 277.9±108.3 μg m^{-3}). Generally, OVOCs are dominant contributors to OFP at suburban (TZ, 225.4 μg m^{-3}) and industrial (XD, 182.1 μg m^{-3}) sites, followed by urban (ZL, 151.9 μg m^{-3}), upwind (CQ, 141.7 μg m^{-3}), and downwind (CD, 100.1 μg m^{-3}) sites. The high levels of OVOCs and their significant contribution to OFP highlights their crucial role in O_3 production.

Based on the OBM simulation, daytime OVOCs primarily originate from photochemical

https://doi.org/10.5194/egusphere-2024-3201
Preprint. Discussion started: 25 November 2024

reactions, while at nighttime, emissions/transport is the main sources. This diurnal pattern is closely related to the cyclical nature of human activities in urban areas (ZL), where stronger human activities such as vehicle emissions in the daytime enhance the secondary generation of OVOCs. Conversely, in industrial and suburban areas (XD, CQ, and TZ), emissions/transports dominate nighttime OVOC levels, leading to higher concentrations at night compared to that at daytime.

Without OVOCs constraint in the OBM, OVOCs are overestimated by 42.1%~126.5% in the Free scenario. The impact of OVOCs constraint on $P(RO_x)$ is most significant at the urban site (ZL) (29.4%), comparable to downwind site (CD) (27.6%), and higher than the industrial site (XD) (17.8%), upwind site (CQ) (15.8%) and suburban site (TZ) (4.7%). In addition, this overestimation of OVOCs in the Free scenario accelerates the reaction of OH with OVOCs and the photolysis of OVOCs, promote the production of RO_2 (6.6%~35.1%) and HO_2 (5.3%~ 20.4%), which in turn leads to an overestimation of O_3 (1.8%~11.9%) during the daytime. However, the reaction rates of OH with OVOCs are overestimated without OVOCs constraint, which leads to underestimation of OH (3.4%~12.7%) and AOC (3.4%~12.7%). Therefore, to minimize the bias of numerical models, particularly in areas with complex anthropogenic activities, it is essential to intensify OVOCs observations and integrate them into numerical models. Such efforts are crucial for refining atmospheric photochemistry simulation, improving the accuracy of O_3 formation predictions, and formulating more effective air quality management strategies for regions experiencing similar pollution challenges.

Author contributions

KZ, XY, RL, JX, QL, LSS, JQL, YNY, FTW and LMY conducted the field measurements. JWD and KZ performed the data analysis and prepared the manuscript with contributions from all

https://doi.org/10.5194/egusphere-2024-3201
Preprint. Discussion started: 25 November 2024

co-authors. KZ, YLF, HC, LH, JNT, YJW and LL reviewed and edited the manuscript. All authors contributed to data interpretation and discussions.

Competing interests

The contact author has declared that none of the authors has any competing interests.

Acknowledgment

This study was financially supported by the National research program for key issues in air pollution control (DQGG202119). This work is supported by Shanghai Technical Service Center of Science and Engineering Computing, Shanghai University.

References

Atkinson, R. and Arey, J.: Atmospheric Degradation of Volatile Organic Compounds, Chem. Rev., 103, 4605–4638, https://doi.org/10.1021/cr0206420, 2003.

Carter, W. P. L.: A detailed mechanism for the gas-phase atmospheric reactions of organic compounds, Atmospheric Environment. Part A. General Topics, 24, 481–518, https://doi.org/10.1016/0960-1686(90)90005-8, 1990.

Carter, W. P. L.: Development of the SAPRC-07 chemical mechanism, Atmos. Environ., 44, 5324–5335, https://doi.org/10.1016/j.atmosenv.2010.01.026, 2010.

Carter, W. P. L. and Heo, G.: Development of revised SAPRC aromatics mechanisms, Atmos. Environ., 77, 404–414, https://doi.org/10.1016/j.atmosenv.2013.05.021, 2013.

Chen, T., Zheng, P., Zhang, Y., Dong, C., Han, G., Li, H., Yang, X., Liu, Y., Sun, J., Li, H., Zhang, X., Li, Y., Wang, W., and Xue, L.: Characteristics and formation mechanisms of atmospheric carbonyls in an oilfield region of northern China, Atmos. Environ., 274, 118958, https://doi.org/10.1016/j.atmosenv.2022.118958, 2022.

Duan, J., Tan, J., Yang, L., Wu, S., and Hao, J.: Concentration, sources and ozone formation potential of volatile organic compounds (VOCs) during ozone episode in Beijing, Atmospheric Research, 88, 25–35, https://doi.org/10.1016/j.atmosres.2007.09.004, 2008.

Edwards, P. M., Brown, S. S., Roberts, J. M., Ahmadov, R., Banta, R. M., deGouw, J. A., Dube, W. P., Field, R. A., Flynn, J. H., Gilman, J. B., Graus, M., Helmig, D., Koss, A., Langford, A. O., Lefer, B. L., Lerner, B. M., Li, R., Li, S.-M., McKeen, S. A., Murphy, S. M., Parrish, D. D., Senff, C. J., Soltis, J., Stutz, J., Sweeney, C., Thompson, C. R., Trainer, M. K., Tsai, C., Veres, P. R., Washenfelder, R. A., Warneke, C., Wild, R. J., Young, C. J., Yuan, B., and Zamora, R.: High winter ozone pollution from carbonyl photolysis in an oil and gas basin, Nature, 514, 351–354, https://doi.org/10.1038/nature13767, 2014.

Elshorbany, Y. F., Steil, B., Bruehl, C., and Lelieveld, J.: Impact of HONO on global atmospheric chemistry calculated with an empirical parameterization in the EMAC model, Atmos. Chem. Phys., 12, 9977–10000, https://doi.org/10.5194/acp-12-9977-2012, 2012.

https://doi.org/10.5194/egusphere-2024-3201
Preprint. Discussion started: 25 November 2024

Emmerson, K. M., Carslaw, N., and Pilling, M. J.: Urban atmospheric chemistry during the PUMA campaign 2: Radical budgets for OH, HO_2 and RO_2, J. Atmos. Chem., 52, 165–183, https://doi.org/10.1007/s10874-005-1323-2, 2005.

Fuchs, H., Tan, Z., Lu, K., Bohn, B., Broch, S., Brown, S. S., Dong, H., Gomm, S., Häseler, R., He, L., Hofzumahaus, A., Holland, F., Li, X., Liu, Y., Lu, S., Min, K.-E., Rohrer, F., Shao, M., Wang, B., Wang, M., Wu, Y., Zeng, L., Zhang, Y., Wahner, A., and Zhang, Y.: OH reactivity at a rural site (Wangdu) in the North China Plain: contributions from OH reactants and experimental OH budget, Atmos. Chem. Phys., 17, 645–661, https://doi.org/10.5194/acp-17-645-2017, 2017.

Geyer, A., Alicke, B., Konrad, S., Schmitz, T., Stutz, J., and Platt, U.: Chemistry and oxidation capacity of the nitrate radical in the continental boundary layer near Berlin, J. Geophys. Res.-Atmos., 106, 8013–8025, https://doi.org/10.1029/2000JD900681, 2001.

Goldan, P. D., Kuster, W. C., Williams, E., Murphy, P. C., Fehsenfeld, F. C., and Meagher, J.: Nonmethane hydrocarbon and oxy hydrocarbon measurements during the 2002 New England Air Quality Study, J. Geophys. Res.-Atmos., 109, D21309, https://doi.org/10.1029/2003JD004455, 2004.

Goliff, W. S., Stockwell, W. R., and Lawson, C. V.: The regional atmospheric chemistry mechanism, version 2, Atmos. Environ., 68, 174–185, https://doi.org/10.1016/j.atmosenv.2012.11.038, 2013.

de Gouw, J. A., Gilman, J. B., Kim, S.-W., Lerner, B. M., Isaacman-VanWertz, G., McDonald, B. C., Warneke, C., Kuster, W. C., Lefer, B. L., Griffith, S. M., Dusanter, S., Stevens, P. S., and Stutz, J.: Chemistry of Volatile Organic Compounds in the Los Angeles basin: Nighttime Removal of Alkenes and Determination of Emission Ratios, J. Geophys. Res.-Atmos., 122, 11843–11861, https://doi.org/10.1002/2017JD027459, 2017.

de Gouw, J. A., Gilman, J. B., Kim, S.-W., Alvarez, S. L., Dusanter, S., Graus, M., Griffith, S. M., Isaacman-VanWertz, G., Kuster, W. C., Lefer, B. L., Lerner, B. M., McDonald, B. C., Rappenglück, B., Roberts, J. M., Stevens, P. S., Stutz, J., Thalman, R., Veres, P. R., Volkamer, R., Warneke, C., Washenfelder, R. A., and Young, C. J.: Chemistry of Volatile Organic Compounds in the Los Angeles Basin: Formation of Oxygenated Compounds and Determination of Emission Ratios, Journal of Geophysical Research: Atmospheres, 123, 2298–2319, https://doi.org/10.1002/2017JD027976, 2018.

Guo, F., Bui, A. A. T., Schulze, B. C., Yoon, S., Shrestha, S., Wallace, H. W., Sakai, Y., Actkinson, B. W., Erickson, M. H., Alvarez, S., Sheesley, R., Usenko, S., Flynn, J., and Griffin, R. J.: Urban core-downwind differences and relationships related to ozone production in a major urban area in Texas, Atmos. Environ., 262, 118624, https://doi.org/10.1016/j.atmosenv.2021.118624, 2021.

Han, Y., Huang, X., Wang, C., Zhu, B., and He, L.: Characterizing oxygenated volatile organic compounds and their sources in rural atmospheres in China, J. Environ. Sci., 81, 148–155, https://doi.org/10.1016/j.jes.2019.01.017, 2019.

Huang, X.-F., Zhang, B., Xia, S.-Y., Han, Y., Wang, C., Yu, G.-H., and Feng, N.: Sources of oxygenated volatile organic compounds (OVOCs) in urban atmospheres in North and South China, Environ. Pollut., 261, 114152, https://doi.org/10.1016/j.envpol.2020.114152, 2020.

Jenkin, M. E., Young, J. C., and Rickard, A. R.: The MCM v3.3.1 degradation scheme for isoprene, Atmos. Chem. Phys., 15, 11433–11459, https://doi.org/10.5194/acp-15-11433-2015, 2015.

Karl, T., Striednig, M., Graus, M., Hammerle, A., and Wohlfahrt, G.: Urban flux measurements reveal a large pool of oxygenated volatile organic compound emissions, Proc. Natl. Acad. Sci. U. S. A., 115, 1186–1191, https://doi.org/10.1073/pnas.1714715115, 2018.

Koss, A. R., de Gouw, J., Warneke, C., Gilman, J. B., Lerner, B. M., Graus, M., Yuan, B., Edwards, P., Brown, S. S., Wild, R., Roberts, J. M., Bates, T. S., and Quinn, P. K.: Photochemical aging of

https://doi.org/10.5194/egusphere-2024-3201
Preprint. Discussion started: 25 November 2024

volatile organic compounds associated with oil and natural gas extraction in the Uintah Basin, UT, during a wintertime ozone formation event, Atmos. Chem. Phys., 15, 5727–5741, https://doi.org/10.5194/acp-15-5727-2015, 2015.

Li, C., Liu, Y., Cheng, B., Zhang, Y., Liu, X., Qu, Y., An, J., Kong, L., Zhang, Y., Zhang, C., Tan, Q., and Feng, M.: A comprehensive investigation on volatile organic compounds (VOCs) in 2018 in Beijing, China: Characteristics, sources and behaviours in response to O_3 formation, Sci. Total Environ., 806, 150247, https://doi.org/10.1016/j.scitotenv.2021.150247, 2022a.

Li, J., Xie, X., Li, L., Wang, X., Wang, H., Jing, S., Ying, Q., Qin, M., and Hu, J.: Fate of Oxygenated Volatile Organic Compounds in the Yangtze River Delta Region: Source Contributions and Impacts on the Atmospheric Oxidation Capacity, Environ. Sci. Technol., 56, 11212–11224, https://doi.org/10.1021/acs.est.2c00038, 2022b.

Li, K., Wang, X., Li, L., Wang, J., Liu, Y., Cheng, X., Xu, B., Wang, X., Yan, P., Li, S., Geng, C., Yang, W., Azzi, M., and Bai, Z.: Large variability of O_3-precursor relationship during severe ozone polluted period in an industry-driven cluster city (Zibo) of North China Plain, J. Clean Prod., 316, 128252, https://doi.org/10.1016/j.jclepro.2021.128252, 2021a.

Li, K., Jacob, D. J., Liao, H., Qiu, Y., Shen, L., Zhai, S., Bates, K. H., Sulprizio, M. P., Song, S., Lu, X., Zhang, Q., Zheng, B., Zhang, Y., Zhang, J., Lee, H. C., and Kuk, S. K.: Ozone pollution in the North China Plain spreading into the late-winter haze season, Proc. Natl. Acad. Sci. U. S. A., 118, e2015797118, https://doi.org/10.1073/pnas.2015797118, 2021b.

Li, M., Zhang, Q., Streets, D. G., He, K. B., Cheng, Y. F., Emmons, L. K., Huo, H., Kang, S. C., Lu, Z., Shao, M., Su, H., Yu, X., and Zhang, Y.: Mapping Asian anthropogenic emissions of non-methane volatile organic compounds to multiple chemical mechanisms, Atmos. Chem. Phys., 14, 5617–5638, https://doi.org/10.5194/acp-14-5617-2014, 2014a.

Li, M., Zhang, Q., Zheng, B., Tong, D., Lei, Y., Liu, F., Hong, C., Kang, S., Yan, L., Zhang, Y., Bo, Y., Su, H., Cheng, Y., and He, K.: Persistent growth of anthropogenic non-methane volatile organic compound (NMVOC) emissions in China during 1990-2017: drivers, speciation and ozone formation potential, Atmos. Chem. Phys., 19, 8897–8913, https://doi.org/10.5194/acp-19-8897-2019, 2019.

Li, X., Rohrer, F., Brauers, T., Hofzumahaus, A., Lu, K., Shao, M., Zhang, Y. H., and Wahner, A.: Modeling of HCHO and CHOCHO at a semi-rural site in southern China during the PRIDE-PRD2006 campaign, Atmos. Chem. Phys., 14, 12291–12305, https://doi.org/10.5194/acp-14-12291-2014, 2014b.

Ling, Z. H., Guo, H., Lam, S. H. M., Saunders, S. M., and Wang, T.: Atmospheric photochemical reactivity and ozone production at two sites in Hong Kong: Application of a Master Chemical Mechanism–photochemical box model, J. Geophys. Res.-Atmos., 119, 10567–10582, https://doi.org/10.1002/2014JD021794, 2014.

Liu, G., Ma, X., Li, W., Chen, J., Ji, Y., and An, T.: Pollution characteristics, source appointment and environmental effect of oxygenated volatile organic compounds in Guangdong-Hong Kong-Macao Greater Bay Area: Implication for air quality management, Sci. Total Environ., 919, 170836, https://doi.org/10.1016/j.scitotenv.2024.170836, 2024.

Liu, Y., Yuan, B., Li, X., Shao, M., Lu, S., Li, Y., Chang, C.-C., Wang, Z., Hu, W., Huang, X., He, L., Zeng, L., Hu, M., and Zhu, T.: Impact of pollution controls in Beijing on atmospheric oxygenated volatile organic compounds (OVOCs) during the 2008 Olympic Games: observation and modeling implications, Atmos. Chem. Phys., 15, 3045–3062, https://doi.org/10.5194/acp-15-3045-2015, 2015.

Liu, Z., Wang, Y., Gu, D., Zhao, C., Huey, L. G., Stickel, R., Liao, J., Shao, M., Zhu, T., Zeng, L., Amoroso, A., Costabile, F., Chang, C.-C., and Liu, S.-C.: Summertime photochemistry during CAREBeijing-2007: RO_x budgets and O_3 formation, Atmos. Chem. Phys., 12, 7737–7752,

https://doi.org/10.5194/egusphere-2024-3201
Preprint. Discussion started: 25 November 2024

https://doi.org/10.5194/acp-12-7737-2012, 2012.

Lou, S., Holland, F., Rohrer, F., Lu, K., Bohn, B., Brauers, T., Chang, C. C., Fuchs, H., Haeseler, R., Kita, K., Kondo, Y., Li, X., Shao, M., Zeng, L., Wahner, A., Zhang, Y., Wang, W., and Hofzumahaus, A.: Atmospheric OH reactivities in the Pearl River Delta - China in summer 2006: measurement and model results, Atmos. Chem. Phys., 10, 11243–11260, https://doi.org/10.5194/acp-10-11243-2010, 2010.

Luecken, D. J., Hutzell, W. T., Strum, M. L., and Pouliot, G. A.: Regional sources of atmospheric formaldehyde and acetaldehyde, and implications for atmospheric modeling, Atmos. Environ., 47, 477–490, https://doi.org/10.1016/j.atmosenv.2011.10.005, 2012.

McDonald, B. C., de Gouw, J. A., Gilman, J. B., Jathar, S. H., Akherati, A., Cappa, C. D., Jimenez, J. L., Lee-Taylor, J., Hayes, P. L., McKeen, S. A., Cui, Y. Y., Kim, S.-W., Gentner, D. R., Isaacman-VanWertz, G., Goldstein, A. H., Harley, R. A., Frost, G. J., Roberts, J. M., Ryerson, T. B., and Trainer, M.: Volatile chemical products emerging as largest petrochemical source of urban organic emissions, Science, 359, 760–764, https://doi.org/10.1126/science.aaq0524, 2018.

Mo, Z., Shao, M., and Lu, S.: Compilation of a source profile database for hydrocarbon and OVOC emissions in China, Atmos. Environ., 143, 209–217, https://doi.org/10.1016/j.atmosenv.2016.08.025, 2016.

Mo, Z., Shao, M., Wang, W., Liu, Y., Wang, M., and Lu, S.: Evaluation of biogenic isoprene emissions and their contribution to ozone formation by ground-based measurements in Beijing, China, Sci. Total Environ., 627, 1485–1494, https://doi.org/10.1016/j.scitotenv.2018.01.336, 2018.

Pfannerstill, E. Y., Arata, C., Zhu, Q., Schulze, B. C., Woods, R., Harkins, C., Schwantes, R. H., McDonald, B. C., Seinfeld, J. H., Bucholtz, A., Cohen, R. C., and Goldstein, A. H.: Comparison between Spatially Resolved Airborne Flux Measurements and Emission Inventories of Volatile Organic Compounds in Los Angeles, Environ. Sci. Technol., 57, 15533–15545, https://doi.org/10.1021/acs.est.3c03162, 2023.

Qin, Z., Xu, B., Zheng, Z., Li, L., Zhang, G., Li, S., Geng, C., Bai, Z., and Yang, W.: Integrating ambient carbonyl compounds provides insight into the constrained ozone formation chemistry in Zibo city of the North China Plain, Environ. Pollut., 324, 121294, https://doi.org/10.1016/j.envpol.2023.121294, 2023.

Qu, H., Wang, Y., Zhang, R., Liu, X., Huey, L. G., Sjostedt, S., Zeng, L., Lu, K., Wu, Y., Shao, M., Hu, M., Tan, Z., Fuchs, H., Broch, S., Wahner, A., Zhu, T., and Zhang, Y.: Chemical Production of Oxygenated Volatile Organic Compounds Strongly Enhances Boundary-Layer Oxidation Chemistry and Ozone Production, Environ. Sci. Technol., 55, 13718–13727, https://doi.org/10.1021/acs.est.1c04489, 2021.

Sarwar, G., Luecken, D., Yarwood, G., Whitten, G. Z., and Carter, W. P. L.: Impact of an updated carbon bond mechanism on predictions from the CMAQ modeling system: Preliminary assessment, J. Appl. Meteorol. Climatol., 47, 3–14, https://doi.org/10.1175/2007JAMC1393.1, 2008.

Shen, L., Jacob, D. J., Zhu, L., Zhang, Q., Zheng, B., Sulprizio, M. P., Li, K., De Smedt, I., Abad, G. G., Cao, H., Fu, T.-M., and Liao, H.: The 2005-2016 Trends of Formaldehyde Columns Over China Observed by Satellites: Increasing Anthropogenic Emissions of Volatile Organic Compounds and Decreasing Agricultural Fire Emissions, Geophys. Res. Lett., 46, 4468–4475, https://doi.org/10.1029/2019GL082172, 2019.

Sindelarova, K., Granier, C., Bouarar, I., Guenther, A., Tilmes, S., Stavrakou, T., Muller, J.-F., Kuhn, U., Stefani, P., and Knorr, W.: Global data set of biogenic VOC emissions calculated by the MEGAN model over the last 30 years, Atmos. Chem. Phys., 14, 9317–9341, https://doi.org/10.5194/acp-14-9317-2014, 2014.

https://doi.org/10.5194/egusphere-2024-3201
Preprint. Discussion started: 25 November 2024

548 Song, J., Saathoff, H., Jiang, F., Gao, L., Zhang, H., and Leisner, T.: Sources of organic gases and
549 aerosol particles and their roles in nighttime particle growth at a rural forested site in southwest
550 Germany, Atmos. Chem. Phys., 24, 6699–6717, https://doi.org/10.5194/acp-24-6699-2024, 2024.

551 Song, M., Li, X., Yang, S., Yu, X., Zhou, S., Yang, Y., Chen, S., Dong, H., Liao, K., Chen, Q., Lu,
552 K., Zhang, N., Cao, J., Zeng, L., and Zhang, Y.: Spatiotemporal variation, sources, and secondary
553 transformation potential of volatile organic compounds in Xi'an, China, Atmos. Chem. Phys., 21,
554 4939–4958, https://doi.org/10.5194/acp-21-4939-2021, 2021.

555 Steiner, A. L., Cohen, R. C., Harley, R. A., Tonse, S., Millet, D. B., Schade, G. W., and Goldstein,
556 A. H.: VOC reactivity in central California: comparing an air quality model to ground-based
557 measurements, Atmos. Chem. Phys., 8, 351–368, https://doi.org/10.5194/acp-8-351-2008, 2008.

558 Stockwell, W. R., Kirchner, F., Kuhn, M., and Seefeld, S.: A new mechanism for regional
559 atmospheric chemistry modeling, J. Geophys. Res.-Atmos., 102, 25847–25879,
560 https://doi.org/10.1029/97JD00849, 1997a.

561 Stockwell, W. R., Kirchner, F., Kuhn, M., and Seefeld, S.: A new mechanism for regional
562 atmospheric chemistry modeling, J. Geophys. Res.-Atmos., 102, 25847–25879,
563 https://doi.org/10.1029/97JD00849, 1997b.

564 Tan, Z., Fuchs, H., Lu, K., Hofzumahaus, A., Bohn, B., Broch, S., Dong, H., Gomm, S., Haeseler,
565 R., He, L., Holland, F., Li, X., Liu, Y., Lu, S., Rohrer, F., Shao, M., Wang, B., Wang, M., Wu, Y.,
566 Zeng, L., Zhang, Y., Wahner, A., and Zhang, Y.: Radical chemistry at a rural site (Wangdu) in the
567 North China Plain: observation and model calculations of OH, HO_2 and RO_2 radicals, Atmos. Chem.
568 Phys., 17, 663–690, https://doi.org/10.5194/acp-17-663-2017, 2017.

569 Tan, Z., Lu, K., Jiang, M., Su, R., Dong, H., Zeng, L., Xie, S., Tan, Q., and Zhang, Y.: Exploring
570 ozone pollution in Chengdu, southwestern China: A case study from radical chemistry to O_3-VOC-
571 NO_x sensitivity, Sci. Total Environ., 636, 775–786, https://doi.org/10.1016/j.scitotenv.2018.04.286,
572 2018a.

573 Tan, Z., Rohrer, F., Lu, K., Ma, X., Bohn, B., Broch, S., Dong, H., Fuchs, H., Gkatzelis, G. I.,
574 Hofzumahaus, A., Holland, F., Li, X., Liu, Y., Liu, Y., Novelli, A., Shao, M., Wang, H., Wu, Y., Zeng,
575 L., Hu, M., Kiendler-Scharr, A., Wahner, A., and Zhang, Y.: Wintertime photochemistry in Beijing:
576 observations of RO_x radical concentrations in the North China Plain during the BEST-ONE
577 campaign, Atmos. Chem. Phys., 18, 12391–12411, https://doi.org/10.5194/acp-18-12391-2018,
578 2018b.

579 Tan, Z., Lu, K., Jiang, M., Su, R., Wang, H., Lou, S., Fu, Q., Zhai, C., Tan, Q., Yue, D., Chen, D.,
580 Wang, Z., Xie, S., Zeng, L., and Zhang, Y.: Daytime atmospheric oxidation capacity in four Chinese
581 megacities during the photochemically polluted season: a case study based on box model simulation,
582 Atmos. Chem. Phys., 19, 3493–3513, https://doi.org/10.5194/acp-19-3493-2019, 2019a.

583 Tan, Z., Lu, K., Hofzumahaus, A., Fuchs, H., Bohn, B., Holland, F., Liu, Y., Rohrer, F., Shao, M.,
584 Sun, K., Wu, Y., Zeng, L., Zhang, Y., Zou, Q., Kiendler-Scharr, A., Wahner, A., and Zhang, Y.:
585 Experimental budgets of OH, HO_2, and RO_2 radicals and implications for ozone formation in the
586 Pearl River Delta in China 2014, Atmos. Chem. Phys., 19, 7129–7150, https://doi.org/10.5194/acp-
587 19-7129-2019, 2019b.

588 Venecek, M. A., Carter, W. P. L., and Kleeman, M. J.: Updating the SAPRC Maximum Incremental
589 Reactivity (MIR) scale for the United States from 1988 to 2010, J. Air Waste Manage. Assoc., 68,
590 1301–1316, https://doi.org/10.1080/10962247.2018.1498410, 2018.

591 Volkamer, R., Sheehy, P., Molina, L. T., and Molina, M. J.: Oxidative capacity of the Mexico City
592 atmosphere - Part 1: A radical source perspective, Atmos. Chem. Phys., 10, 6969–6991,
593 https://doi.org/10.5194/acp-10-6969-2010, 2010.

https://doi.org/10.5194/egusphere-2024-3201
Preprint. Discussion started: 25 November 2024

Wang, W., Yuan, B., Peng, Y., Su, H., Cheng, Y., Yang, S., Wu, C., Qi, J., Bao, F., Huangfu, Y., Wang, C., Ye, C., Wang, Z., Wang, B., Wang, X., Song, W., Hu, W., Cheng, P., Zhu, M., Zheng, J., and Shao, M.: Direct observations indicate photodearadable oxygenated volatile organic compounds (OVOCs) as larger contributors to radicals and ozone production in the atmosphere, Atmos. Chem. Phys., 22, 4117–4128, https://doi.org/10.5194/acp-22-4117-2022, 2022.

Wolfe, G. M., Marvin, M. R., Roberts, S. J., Travis, K. R., and Liao, J.: The Framework for 0-D Atmospheric Modeling (F0AM) v3.1, Geosci. Model Dev., 9, 3309–3319, https://doi.org/10.5194/gmd-9-3309-2016, 2016.

Wu, Y., Fan, X., Liu, Y., Zhang, J., Wang, H., Sun, L., Fang, T., Mao, H., Hu, J., Wu, L., Peng, J., and Wang, S.: Source apportionment of VOCs based on photochemical loss in summer at a suburban site in Beijing, Atmos. Environ., 293, 119459, https://doi.org/10.1016/j.atmosenv.2022.119459, 2023.

Xia, S.-Y., Wang, C., Zhu, B., Chen, X., Feng, N., Yu, G.-H., and Huang, X.-F.: Long-term observations of oxygenated volatile organic compounds (OVOCs) in an urban atmosphere in southern China, 2014-2019, Environ. Pollut., 270, 116301, https://doi.org/10.1016/j.envpol.2020.116301, 2021.

Xuan, H., Zhao, Y., Ma, Q., Chen, T., Liu, J., Wang, Y., Liu, C., Wang, Y., Liu, Y., Mu, Y., and He, H.: Formation mechanisms and atmospheric implications of summertime nitrous acid (HONO) during clean, ozone pollution and double high-level $PM_{2.5}$ and O_3 pollution periods in Beijing, Sci. Total Environ., 857, 159538, https://doi.org/10.1016/j.scitotenv.2022.159538, 2023.

Xue, L., Wang, T., Louie, P. K. K., Luk, C. W. Y., Blake, D. R., and Xu, Z.: Increasing External Effects Negate Local Efforts to Control Ozone Air Pollution: A Case Study of Hong Kong and Implications for Other Chinese Cities, Environ. Sci. Technol., 48, 10769–10775, https://doi.org/10.1021/es503278g, 2014.

Xue, L., Gu, R., Wang, T., Wang, X., Saunders, S., Blake, D., Louie, P. K. K., Luk, C. W. Y., Simpson, I., Xu, Z., Wang, Z., Gao, Y., Lee, S., Mellouki, A., and Wang, W.: Oxidative capacity and radical chemistry in the polluted atmosphere of HongKong and Pearl River Delta region: analysis of a severe photochemical smog episode, Atmos. Chem. Phys., 16, 9891–9903, https://doi.org/10.5194/acp-16-9891-2016, 2016.

Yang, C., Yao, N., Xu, L., Chen, G., Wang, Y., Fan, X., Zhou, P., Clusius, P., Tham, Y. J., Lin, Z., Chen, Y., Li, M., Hong, Y., and Chen, J.: Molecular Composition of Anthropogenic Oxygenated Organic Molecules and Their Contribution to Organic Aerosol in a Coastal City, Environ. Sci. Technol., 57, 15956–15967, https://doi.org/10.1021/acs.est.3c03244, 2023.

Yang, M., Beale, R., Liss, P., Johnson, M., Blomquist, B., and Nightingale, P.: Air-sea fluxes of oxygenated volatile organic compounds across the Atlantic Ocean, Atmos. Chem. Phys., 14, 7499–7517, https://doi.org/10.5194/acp-14-7499-2014, 2014.

Yang, X., Xue, L., Wang, T., Wang, X., Gao, J., Lee, S., Blake, D. R., Chai, F., and Wang, W.: Observations and Explicit Modeling of Summertime Carbonyl Formation in Beijing: Identification of Key Precursor Species and Their Impact on Atmospheric Oxidation Chemistry, J. Geophys. Res.-Atmos., 123, 1426–1440, https://doi.org/10.1002/2017JD027403, 2018.

Yarwood, G., Rao, S., Way, R., Yocke, M., Whitten, G. Z., and Reyes, S.: Deborah Luecken U.S. Environmental Protection Agency Research Triangle Park, NC 27703, 2005.

Yarwood, G., Jung, J., Whitten, G. Z., Heo, G., Mellberg, J., and Estes, M.: Updates to the Carbon Bond mechanism for version 6 (CB6), 2010.

Zhang, K., Huang, L., Li, Q., Huo, J., Duan, Y., Wang, Y., Yaluk, E., Wang, Y., Fu, Q., and Li, L.: Explicit modeling of isoprene chemical processing in polluted air masses in suburban areas of the

https://doi.org/10.5194/egusphere-2024-3201
Preprint. Discussion started: 25 November 2024

640 Yangtze River Delta region: radical cycling and formation of ozone and formaldehyde, Atmos.
641 Chem. Phys., 21, 5905–5917, https://doi.org/10.5194/acp-21-5905-2021, 2021a.

642 Zhang, K., Duan, Y., Huo, J., Huang, L., Wang, Y., Fu, Q., Wang, Y., and Li, L.: Formation
643 mechanism of HCHO pollution in the suburban Yangtze River Delta region, China: A box model
644 study and policy implementations, Atmos. Environ., 267, 118755,
645 https://doi.org/10.1016/j.atmosenv.2021.118755, 2021b.

646 Zhang, Z., Sun, Y., and Li, J.: Characteristics and sources of VOCs in a coastal city in eastern China
647 and the implications in secondary organic aerosol and O_3 formation, Sci. Total Environ., 887,
648 164117, https://doi.org/10.1016/j.scitotenv.2023.164117, 2023.

649 Zheng, Z., Li, K., Xu, B., Dou, J., Li, L., Zhang, G., Li, S., Geng, C., Yang, W., Azzi, M., and Bai,
650 Z.: O_3-precursor relationship over multiple patterns of timescale: a case study in Zibo, Shandong
651 Province, China, Atmos. Chem. Phys., 23, 2649–2665, https://doi.org/10.5194/acp-23-2649-2023,
652 2023.

653 Zhou, J., Zhang, C., Liu, A., Yuan, B., Wang, Y., Wang, W., Zhou, J.-P., Hao, Y., Li, X.-B., He, X.,
654 Song, X., Chen, Y., Yang, S., Yang, S., Wu, Y., Jiang, B., Huang, S., Liu, J., Peng, Y., Qi, J., Deng,
655 M., Zhong, B., Huangfu, Y., and Shao, M.: Measurement report: Vertical and temporal variability
656 in the near-surface ozone production rate and sensitivity in an urban area in the Pearl River Delta
657 region, China, Atmos. Chem. Phys., 24, 9805–9826, https://doi.org/10.5194/acp-24-9805-2024,
658 2024.

659 Zhu, J., Wang, S., Wang, H., Jing, S., Lou, S., Saiz-Lopez, A., and Zhou, B.: Observationally
660 constrained modeling of atmospheric oxidation capacity and photochemical reactivity in Shanghai,
661 China, Atmos. Chem. Phys., 20, 1217–1232, https://doi.org/10.5194/acp-20-1217-2020, 2020.

662